Radiolysis to knock-on damage transition in zeolites under electron beam irradiation

O. Ugurlu,[1] J. Haus,[2] A. A. Gunawan,[2] M. G. Thomas,[3] S. Maheshwari,[2] M. Tsapatsis,[2] and K. A. Mkhoyan[2,*]

[1]*Characterization Facility, University of Minnesota, Minneapolis, Minnesota 55455, USA*
[2]*Department of Chemical Engineering and Materials Science, University of Minnesota, Minneapolis, Minnesota 55455, USA*
[3]*Cornell Center for Materials Research, Cornell University, Ithaca, New York 14853, USA*

The electron-beam-induced damage in a zeolite under 60–200 keV energy beam irradiation has both radiolitic and knock-on components and can be described by linear superposition of these two processes. Theoretical predictions supported by experiments at 60 keV suggest that for electron beam energies smaller than 70 keV, the damage to the specimen follows a radiolitic path. For energies larger than 200 keV, knock-on based sputtering of the material will dominate, while considerable radiolitic movement of the atoms will still be present.

Elastic and inelastic scattering of energetic electrons in specimens are essential for imaging and spectroscopy in transmission electron microscopy (TEM). They are also responsible for electron-beam-induced alterations of specimens limiting quantitative analysis. The most common damage mechanisms can be classified under knock-on damage and radiolysis.[1,2] Every sample is subject to knock-on damage if the energy of incident electrons is high enough to overcome the threshold energy of atomic sputtering.[3,4] Radiolysis, on the other hand, introduces atomic displacements in a solid by converting excitonic energies generated during incident-probe–atomic-electron interactions into momentum by forming a Frankel pair.[5] For radiolysis, the energy stored in an exciton should be as large as the energy necessary for atomic displacement, and the relaxation time for the exciton should be long enough ($\gtrsim 1$ ps) so that mechanical relaxation of the atoms can lead to bonding instabilities. As a result, induced atomic displacement is primarily observed in ice, organics, halides, and silicates.[1]

While it is expected that many materials should be susceptible to both types of electron beam damage at high electron energies ($\gtrsim 100$ keV), there is no such reported case. The occurring damage is found to be either radiolitic or knock-on. Silicate-base materials have been shown to be altered by either damage mechanisms: Hobbs *et al.*[6] and Ihui *et al.*[7] reported radiolysis driven crystalline-to-amorphous transformation in α quartz, while Chen *et al.*[8] measured mass loss in amorphous SiO_2 due to knock-on damage. This raises a question of whether these two mechanisms can be considered independent, and if the dominance of one is due to a difference in damage rates *or* if the presence of one mechanism fundamentally affects the other; for example, the presence of knock-on scatterings changes the excitonic states critical for radiolysis.

In this Brief Report, we show that in the case of a certain zeolite, for a wide range of incident electron energies, both knock-on and radiolitic electron-beam damage mechanisms are active, and a linear superposition of these two processes, characteristic for independent processes, can be used to evaluate the total rate of the damage. Experimental high-resolution imaging and electron energy loss spectroscopy (EELS) studies presented here and a comparison with theoretical damage cross sections indicate that when electron beam energy is smaller than 70 keV, only radiolysis is active, and when it is larger than 70 keV, both mechanisms contribute. These results are of particular significance because an understanding of electron

beam damage in zeolites[9–12] could improve their structure identification.[13–15]

The aluminosilicate zeolite MCM-22 (framework type MWW[16]) formed by calcination of a layered precursor,[17] MCM-22(P), with 2.5-nm-thick layers and a Si/Al ratio of 46.7, has been used in this study. Electron transparent samples were prepared by sonication of small particles for about 5 min in isopropanol, which were picked up by a standard holey-carbon TEM grid. The experiments were carried out in two different TEM's: an FEI Tecnai G2 F-30 300 kV scanning and transmission electron microscope ((S)TEM) equipped with a Schottky field emission gun, S-twin lens, Gatan Enfina-1000 energy loss spectrometer, and low-angle and high-angle annular dark field (ADF) detectors, and a Nion aberration-corrected dedicated Ultra-STEM.[18]

During knock-on damage, an incident energetic electron of the probe in a direct collision transfers a significant amount of energy to the atoms of the specimen, which can be sufficient to remove an atom from its site or sputter it from the surface.[19,20] The maximum energy that can be transferred to an atom in a collision is[3,4]

$$E_{max} = \frac{2E(E + 2m_0c^2)}{M_0c^2}, \qquad (1)$$

where E is the energy of incident electrons, M_0 is the mass of the atom, and $m_0c^2 = 511$ keV is the rest energy of the electron. This equation also provides the threshold energy, $E_{th}^{(1)}$, that incident electrons must have to be able to displace or sputter atoms from a site in a solid. The probabilities for vacancy-enhanced displacement and surface sputtering, which are the two dominating processes for knock-on damage, can be described using the Mott cross sections.[3,21] The Mott cross section for surface sputtering (which is the limiting mechanism) for a relativistic incident electron can be expressed as[4,22]

$$\sigma_k(E) = \pi \left(\frac{Ze^2}{m_0c^2} \right)^2 \frac{1 - \beta^2}{\beta^4} [(\xi - 1) - \beta^2 \ln(\xi)$$
$$+ \pi \alpha \beta \{ 2(\xi^{\frac{1}{2}} - 1) - \ln(\xi) \}], \qquad (2)$$

where Z is the atomic number, $\alpha = Z/137$, $\xi = E_{max}/E_{th}^{(1)}$, and $\beta = v/c = \sqrt{1 - (1 + E/m_0c^2)^{-2}}$. The Si-O binding energy in silicates is about 5–5.5 eV/bond,[23] resulting in the threshold energies for oxygen and silicon atoms in the zeolite to be about 70 and 115 eV, respectively. The dependence of
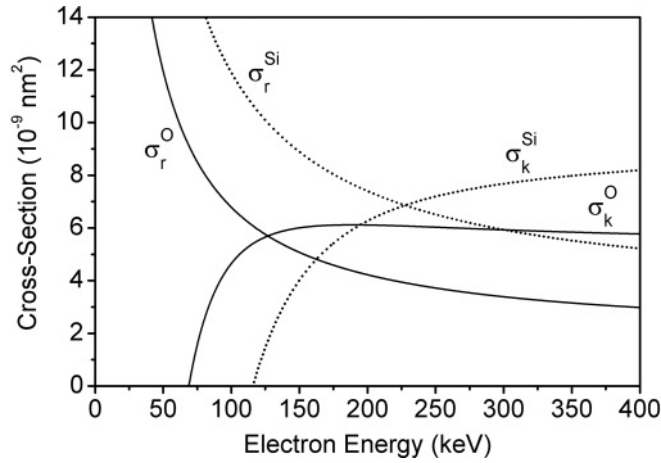
FIG. 1. Calculated crosssections for radiolytic movement and knock-on surface sputtering for silicon and oxygen atoms in the MCM-22 zeolite as a function of incident electron energy.

the cross sections of knock-on damage on incident electron energy for oxygen and silicon atoms is presented in Fig. 1, where $\sigma_k(E)$ has a nonzero value at energies $E > E_{\text{th}}^{(1)}$. This suggests that in microscopes with a beam energy lower than 65 keV, knock-on damage should not occur. Since the fraction of Al in the sample is small, its presence is neglected in the modeled structure.

The cross section of radiolytic movement of atoms in a specimen for a relativistic incident electron is given as[1]

$$\sigma_r(E) = \pi \left(\frac{Ze^2}{m_0 c^2} \right) \frac{2e^2}{E_{th}^{(2)} \beta^2} \times \zeta, \tag{3}$$

where $E_{\text{th}}^{(2)}$ is the threshold energy that must be transferred to the electrons of the atom to produce atomic movement. It is defined by bond strength and coordination number of the atom within the specimen. The efficiency factor ζ in Eq. (3) in silicates is $\zeta \simeq 10^{-4}$[1]. The calculated cross sections for the radiolitic movement of silicon and oxygen atoms in the zeolite are presented in Fig. 1.

A series of conventional high-resolution bright-field TEM images of MCM-22 zeolite were collected using FEI-(S)TEM. They were recorded with 5-s intervals at four accelerating voltages: 60, 80, 100, and 200 kV. The electron beam current, measured using the drift tube of the EELS with the magnet switched off, was 0.14 nA during acquisition of all the images. To avoid the effects of specimen thickness on the damage rate, data from samples with similar thicknesses were selected for further analysis. The thickness of each sample was measured using the ratios of the intensities of the single plasmon loss to the zero loss: $t = [I_{\text{pl}}/I_0]\lambda_{\text{pl}} = 0.07\lambda_{\text{pl}}$, where λ_{pl} is the mean free path of plasmon generation.[24,25] The estimated thickness was about 7.5 ± 1 nm.

Fast Fourier transforms (FFT) of the high-resolution images were calculated to evaluate electron-beam-induced damage. The intensity of the spots, I_c, corresponding to periodic fringes in the image, and the rings, I_a, corresponding to an amorphous layer were obtained from the FFT of each image [see Figs. 2(a)–2(f)]. To estimate the damage rates, the ratio $R = (I_c - I_a)/I_a$, which represents a degradation
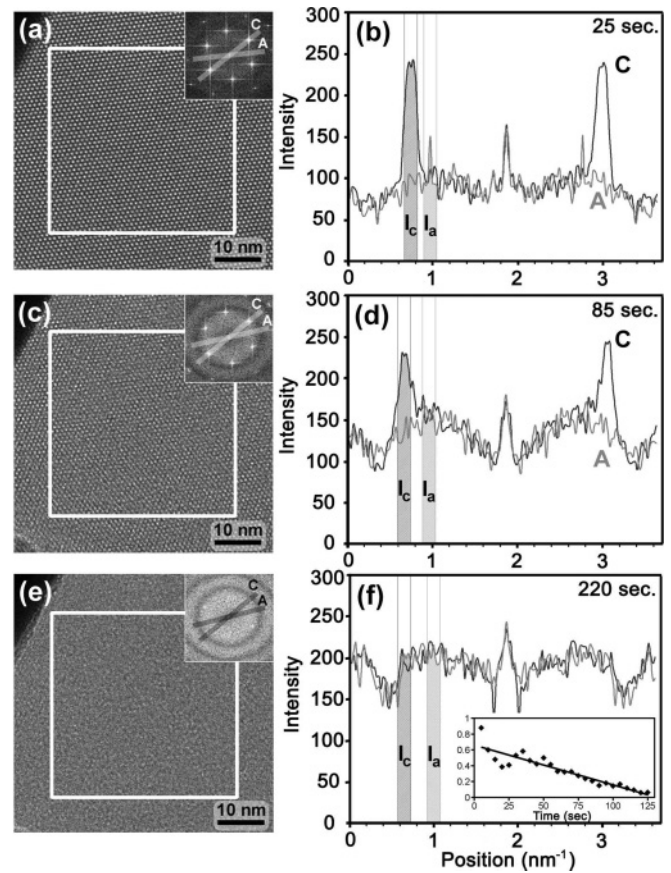

FIG. 2. (a) High-resolution TEM image of MCM-22 zeolite recorded after 25 s of 200 keV electron beam exposure. The inset at the top-right corner is FFT obtained from the highlighted area in the image. (b) Two line scans from the FFT shown in (a) labeled "A" and "C." (c),(d) Same area of the sample after 85 s of beam exposure. (e),(f) The area after 220 s of beam exposure. The inset in (f) is an evaluation of the ratio $R = (I_c - I_a)/I_a$ as a function of exposure time with linear fit.

of the crystal structure of the sample from crystalline to amorphous, was evaluated.[26] Then, the slope of the linear fit to the data set of the decaying ratio, R, as a function of time was used as a damage rate [see the inset in Fig. 2(f)]. The summary of damage rates obtained for incident beams with 60, 80, 100, and 200 keV energy electrons is presented in Fig. 3. For comparison with theoretical predictions, the data were fitted to the total damage cross-section function combining both knock-on and radiolitic scattering processes, $f(E) = A\sigma_{\text{Total}}^{\text{Si-O}}(E) = A[\sigma_k^{\text{ave}}(E) + \sigma_r^{\text{ave}}(E)]$. A single fitting parameter, A, incorporates the incident beam current density and the crystal-to-amorphous transition factor. The average for [SiO$_2$] unit cross sections were used for the sample. The remarkable correlation of the theory and experiment on damage behavior suggests that indeed both damage mechanisms are present during degradation of the zeolite sample when it is exposed to an electron beam with an energy larger than 70 keV.

To confirm these observations, EELS measurements were conducted under the same conditions as imaging with a 200 keV electron beam. EELS spectra of Si $L_{2,3}$ and O K edges were recorded simultaneously with 10-s intervals and 4-s acquisition time from a 5×10^3 nm^2 area of the sample
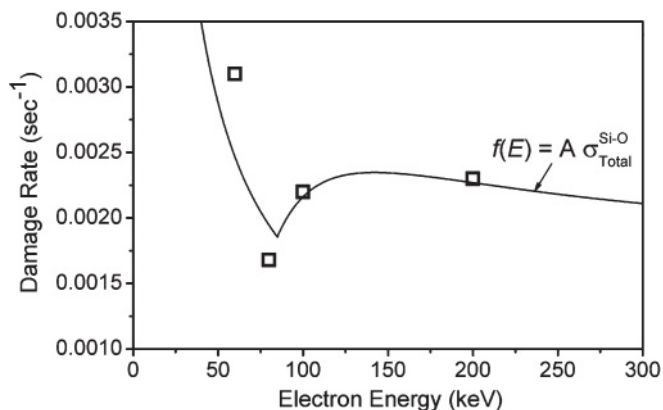
FIG. 3. Caparison of the measured degradation rate in MCM-22 zeolite with calculated total cross section, $\sigma_{\text{Total}}^{\text{Si-O}}(E)$, that includes both radiolysis and knock-on damage mechanisms.

as the crystal structure of the specimen was degrading under electron beam exposure. The integrated intensities of both Si $L_{2,3}$ and O K edges were calculated after standard background subtraction[20,24] and plotted as a function of beam exposure time (Fig. 4). The strong reduction of the number of Si and O atoms from the exposed area is an indication that considerable knock-on-based sputtering of the material is taking place at 200 keV, which is consistent with theoretical predictions (see Figs. 1 and 3).

For damage with 60 keV electrons, a Nion aberration-corrected STEM was used to irradiate the samples and record ADF images. Figures 5(a) and 5(b) show high-resolution ADF images of a layer of MCM-22 zeolite (c axis of the sample was oriented parallel to the incident beam) before and after beam damage. While the loss of crystal structure is apparent, it is not clear that mass loss has taken place. The ADF intensity, I_{ADF}, which is proportional to the number of atoms in the exposed area and the average atomic number (Z) of the sample,[27] was calculated before and after beam damage. The ratio of the ADF intensities obtained from entire images, $I_{\text{ADF}}^{\text{before}}/I_{\text{ADF}}^{\text{after}} = 0.99$,
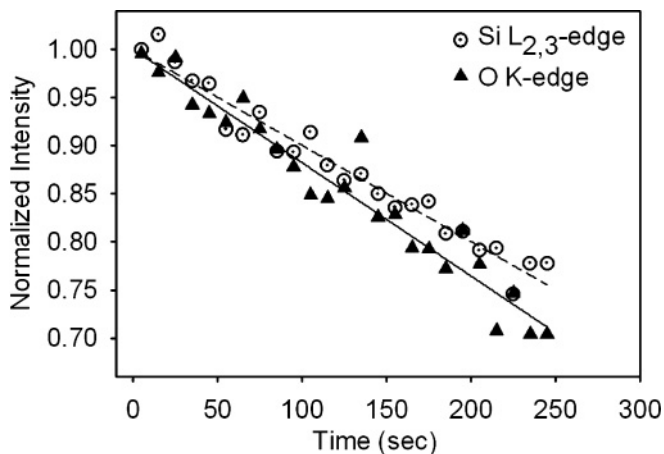

FIG. 4. Measured integrated intensity of the Si $L_{2,3}$ and O K edge EELS spectra as a function of beam exposure time. Starting from edge onset, a 20 eV energy range was used for integration and the results were normalized to the initial spectrum. A 200 keV electron beam was used here.
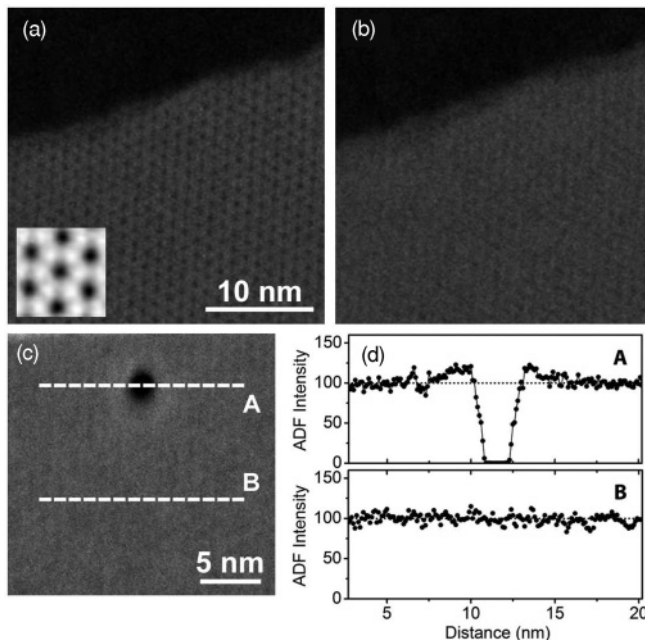

FIG. 5. High-resolution ADF-STEM image of MCM-22 zeolite recorded using 60 keV aberration-corrected STEM before the damage. The inset at the bottom corner is a portion of the same image after statistical improvement. (b) The sample in (a) after 35 s of beam exposure with 40 pA beam current. (c) ADF image of another area after hole formation under an intensive point beam. (d) Two line scans from the image in (c).

indicates that atomic sputtering is not an active scattering process, therefore confirming that radiolysis is the damage mechanism at 60 keV.

To estimate the range of atomic movements in zeolites initiated by radiolysis, the STEM probe was held at one point on the sample for about 10 s to form a hole. A low-magnification ADF image of the area was taken right after [see Fig. 5(c)]. Increased intensity in ADF image in areas around the edges of the hole is due to an accumulation of additional material from the irradiated "hole" area. A line scan obtained from the image across the hole is compared with a similar line scan obtained from the nonirradiated nearby area, and the results are shown in Figs. 5(c) and 5(d). It can be seen that radiolysis in this zeolite produces about 2–3 nm mass displacement.

In conclusion, we observed that electron-beam-induced damage in zeolite at a moderate 60–200 keV electron energy range, typical for most TEM's, has both radiolitic and knock-on components and can be described by a linear superposition of these two processes typical of independent processes. Experimental observations supported by theoretical predictions, based on scattering cross sections, suggest that for the electron beam energies smaller than 70 keV, the damage follows only a radiolitic path. However, for energies bigger than 200 keV, knock-on-based sputtering of material from the surface is expected to be dominant, while considerable radiolitic movement of the atoms will still be present. It was also observed that during radiolysis, mass displacement is about 2–3 nm. The results also suggest that operating the TEM with an 80 keV electron beam will minimize the beam

damage in similar zeolites. These results also suggest that both radiolitic and knock-on damage mechanisms should be present in many silicates, including different crystalline or amorphous forms of SiO_2 sharing similar ($\sim$5 eV) atomic bonding energies. We believe that insufficient analytical capabilities in early TEM's prevented Hobbs *et al.*,[6] Ihui *et al.*,[7] and Chen *et al.*[8] from detecting both damage mechanisms.

*mkhoyan@umn.edu

[1]L. W. Hobbs, *Introduction to Analytical Electron Microscopy*, edited by J. J. Hren, J. I. Goldstein, and D. C. Joy (Scanning Microscopy International, Chicago, 1979), p. 437; *Scanning Microscopy Supplement 4*, edited by J. Schou, P. Kruit, and D. E. Newbury (Scanning Microscopy International, Chicago, 1990), p. 171.

[2]L. Reimer and H. Kohl, *Transmission Electron Microscopy: Physics of Image Formation*, 5th ed. (Springer, Berlin, 2008).

[3]N. F. Mott, Proc. R. Soc. London, Ser. A **135**, 429 (1932).

[4]C. R. Bradley, Report No. ANL-88-48 (1988).

[5]M. N. Kabler and R. T. Williams, Phys. Rev. B **18**, 1948 (1978).

[6]L. W. Hobbs and M. R. Pascucci, J. Phys. (Paris) **41**, 237 (1980); M. R. Pascucci, J. L. Hutchison, and L. W. Hobbs, Radiat. Eff. **74**, 219 (1983).

[7]H. Inui, H. Mori, T. Sakata, and H. Fujita, J. Non-Cryst. Solids **116**, 1 (1990).

[8]G. S. Chen, C. B. Boothroyd, and C. J. Humphreys, Philos. Mag. A **78**, 491 (1998).

[9]R. Csencsits and R. Gronsky, Zeolites **8**, 122 (1988).

[10]M. M. J. Treacy and J. M. Newsam, Ultramicroscopy **23**, 411 (1987).

[11]L. A. Bursill, E. A. Lodge, and J. M. Thomas, Nature (London) **286**, 111 (1980).

[12]Y. Yokota, H. Hashimotoa, and T. Yamaguchi, Ultramicroscopy **54**, 207 (1994).

[13]F. Gramm, C. Baerlocher, L. B. McCuser, S. J. Warrender, P. A. Wright, B. Han, S. B. Hong, Z. Liu, T. Ohsuna, and O. Terasaki, Nature (London) **444**, 79 (2006).

[14]J. Ruan, P. Wu, B. Slater, and O. Terasaki, Angew. Chem. Int. Ed. **44**, 6719 (2005).

[15]P. Wu, J. Ruan, L. Wang, L. Wu, Y. Wang, Y. Liu, W. Fan, M. He, O. Terasaki, and T. Tatsumi, J. Am. Chem. Soc. **130**, 8178 (2008).

[16]Ch. Baerlocher, L. B. McCusker, and D. H. Olson, *Atlas of Zeolite Framework Types* (Elsevier, Amsterdam, 2007).

[17]M. E. Leonowicz, J. A. Lawton, S. L. Lawton, and M. K. Rubin, Science **264**, 1910 (1994).

[18]D. A. Muller, L. F. Kourkoutis, M. Murfitt, J. H. Song, H. Y. Hwang, J. Silcox, N. Dellby, and O. L. Krivanek, Science **319**, 1073 (2008).

[19]D. L. Medlin, L. E. Thomas, and D. G. Howitt, Ultramicroscopy **29**, 228 (1989).

[20]K. A. Mkhoyan and J. Silcox, Appl. Phys. Lett. **82**, 859 (2003).

[21]H. Feshbach, Phys. Rev. **103**, 1597 (1956).

[22]W. A. McKinley and H. Feshbach, Phys. Rev. **74**, 1759 (1948).

[23]D. M. Teter, G. V. Gibbs, M. B. Boisen, D. C. Allan, and M. P. Teter, Phys. Rev. B **52**, 8064 (1995).

[24]R. Egerton, *Electron Energy Loss Spectroscopy in the Electron Microscope* (Plenum, New York, 1996).

[25]K. A. Mkhoyan, T. Babinec, S. E. Maccagnano, E. J. Kirkland, and J. Silcox, Ultramicroscopy **107**, 345 (2007).

[26]The analysis is limited by inherent difference between actual fractions of crystalline and amorphous portions of the specimen and their visibility in high-resolution TEM images, which can be 20%.

[27]S. J. Pennycook and L. A. Boatner, Nature (London) **336**, 565 (1988); S. J. Pennycook and D. E. Jesson, Ultramicroscopy **37**, 14 (1991).